University of Birmingham

Research at Birmingham

A Wideband Array Antenna With 1-Bit Digital-Controllable Radiation Beams

Hu, Jun; Wang, Yi; Hao, Zhang-Cheng

Document Version
Publisher's PDF, also known as Version of record

Link to publication on Research at Birmingham portal

A Wideband Array Antenna With 1-Bit Digital-Controllable Radiation Beams

JUN HU[1], **(Student Member, IEEE), ZHANG-CHENG HAO**[1], **(Senior Member, IEEE),
AND YI WANG**[2], **(Senior Member, IEEE)**
[1]State Key Laboratory of Millimeter Waves, Southeast University, Nanjing 210096, China
[2]Department of Electronic, Electrical and System Engineering, University of Birmingham, Edgbaston B15 2TT, U.K.

Corresponding author: Zhang-Cheng Hao (zchao@seu.edu.cn)

ABSTRACT In this paper, we propose a 4×4 low-profile wideband patch array antenna with radiation pattern agility. The digital-controllable antenna element is composed of a square driven patch, a 2×2 parasitic patch array, and two switchable feeding ports, which are connected to a designed single-pole double-throw switch. Due to the symmetrical structure, individual excitation at the two feeding ports produces a 180° phase difference, giving rise to two basic digital elements of "0" and "1," respectively. By switching the feeding ports for all antenna elements using a micro-controller unit, the radiation beam of the 4×4 array antenna can be dynamically reconfigured. To validate the proposed concept, a prototype operating at 5.7 GHz with an overall size of $3.42\lambda_0 \times 3.42\lambda_0 \times 0.069\lambda_0$ (λ_0 is the free-space wavelength at 5.7 GHz) was fabricated and measured. The measured 10-dB return loss bandwidths for all the states cover the frequency band of 5.12–6.32 GHz. The simulated and measured results show close agreement, which proves the powerful dynamical beam manipulation capability of the proposed array antenna.

INDEX TERMS Electronic beam switching, low profile, wideband, stacked patch structure, digital-controllable, array antenna.

I. INTRODUCTION

Compact and multifunctional antenna is one of the key components of the rapidly developing 5G wireless system, which is required to have the ability to provide multiple radiation beams and switchable operating bandwidths. In recent years, reconfigurable antennas, capable of switching operating frequency [1], polarization [2], [3], radiation pattern [4]–[6], or combinations of the above [7], have attracted extensive attention from 5G wireless systems. In particular, pattern reconfigurable antennas [8]–[10], with the ability to dynamically switch radiation beam, have the advantages of avoiding interference of noise sources, improving security, and enhancing system performance.

Recently, a number of beam switchable antennas [11]–[22] have been proposed based on different techniques. With relatively narrow bandwidths, good beam-switching capability has been demonstrated in [11] and [12] using coaxial feeding or three-bit digital switch. Reconfigurable reflectarray [15], [16] and transmitarray [17], [18] have been developed with high gains. In [16], a dual-frequency 1-bit antenna element was used in a 1600-element reconfigurable

reflectarray with excellent beam scanning performance. In [18], a 400-element reconfigurable transmitarray in X-band was presented to synthesize monopulse radiation patterns for radar applications. More recently, some digitally coding metasurfaces [19]–[21] were proposed to dynamically manipulate far-field beams by using p-i-n diodes. Compared to conventional phased arrays, the technique of using p-i-n diodes to adjust the scattering electromagnetic waves offers an effective alternative to reconfigure the radiation beam with low cost and low weight [15]–[21], but at a cost of radiation performance in terms of side lobe level, scanning resolution and scanning range. On the other hand, compared with conventional switched beam antennas [8], [11]–[14], the coding technique using p-i-n diodes [15]–[21] can provide more switching radiation states. Hence, for applications in 5G internet-of-thing (IoT) and cellular systems which require low cost and dynamically switched multiple beams, the coding technique could be a very good choice.

In our previous work, a 2×2 low profile wideband pattern reconfigurable stacked patch antenna array with four switchable beams was briefly demonstrated [22] using four

single-pole-double-throw (SPDT) switches. This paper extends the idea in [22] with a wider operating bandwidth and an enhanced beam manipulation capability by using digital controlling technique [15]–[21] for a 4 × 4 array. A number of radiation beams including sum-, quad-, as well as difference-beams in different directions can be realized in a wide frequency band by adjusting the coding sequence. Due to the symmetrical structure of the radiation element, individual excitation at the two ports can cause a 180° phase difference over the broad operating frequency band. So, the two symmetrical ports can be used to mimic the two basic digital elements of '0' and '1', respectively, by using p-i-n diodes. This paper is organized as follows. The operational scheme and detailed design of the proposed array antenna are presented in Section II, where multiple radiation beams under different coding sequences are demonstrated with simulation results. In Section III, experiments are performed to validate the designed array antenna prototype. Finally, conclusions are drawn in Section IV.
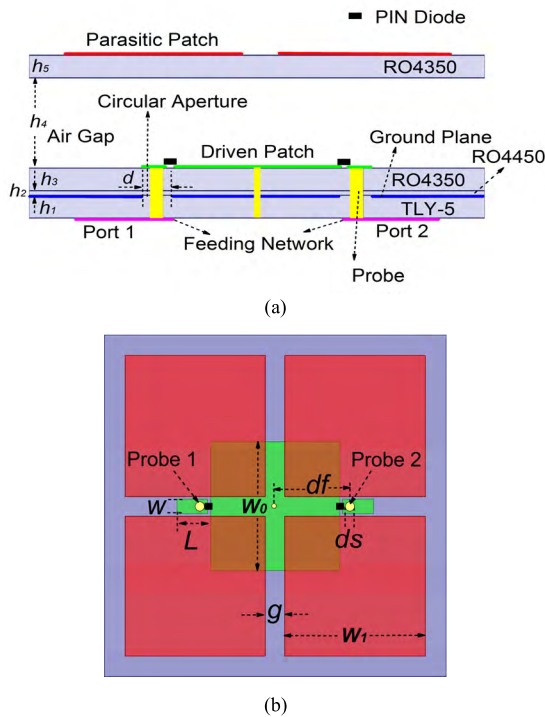

FIGURE 1. Geometrical configuration of the proposed wideband 1-bit antenna element. (a) Side view. (b) Top view. (w_1=14.6mm, g=2.2mm, w_0=13.4mm, W=1.5mm, L=3.5mm, df=7.8mm, ds=1mm, d= 1.4mm, h_1=0.508mm, h_2=0.1mm, h_3=0.508mm, h_4=2mm, h_5=0.508mm)

II. ARRAY ANTENNA DESIGN

A. 1-BIT ANTENNA ELEMENT

The geometrical configuration of the proposed 1-bit digital antenna element and the detailed dimensions are shown in Fig. 1. The proposed antenna element is composed of three layers: the parasitic patch layer, the driven patch layer, and the feeding network layer. These are designed on two 0.508-mm

thick RO4350 substrates (ε_r = 3.66 and tanδ = 0.004 at 10 GHz), and a 0.508-mm thick TLY-5 substrate (ε_r = 2.2 and tanδ = 0.0009 at 10 GHz). The driven patch layer and the feeding network layer are joined together using a piece of bonding film, which is a 0.1-mm thick RO4450 substrate (ε_r = 3.48 and tanδ = 0.004 at 10 GHz). The driven patch layer consists of a square patch with a width of w_0, and two switchable feeding ports. The parasitic patch layer is comprised of four square patches. The length of the four parasitic patches and the gap between adjacent patches are denoted by w_1 and g, respectively. The height of substrates and the air gap are h_1, h_2, h_3 and h_5, as shown in Fig. 1(a). The driven patch is fed by a probe through a microstrip stub with a dimension of $W \times L$. The diameters of the circular aperture at the ground plane and the feeding probe are d and ds, respectively.

The initial sizes of the square driven patch and the parasitic patches are determined by the following empirical formula [2]:

$$w0 = w1 = \frac{\lambda 0}{2\sqrt{\varepsilon_r}} \tag{1}$$

where λ_0 is the free-space wavelength at the operation frequency and ε_r is the relative dielectric constant of the substrate.
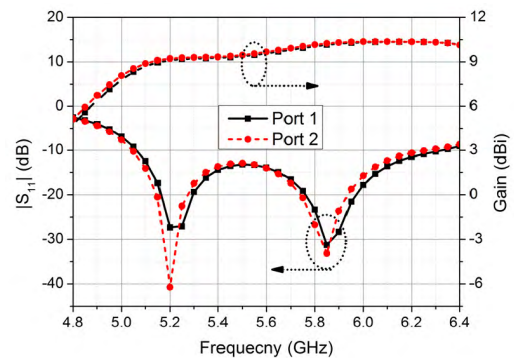

FIGURE 2. Simulated return losses and gains of the designed antenna element from different feeding ports.

The proposed antenna is designed and optimized by the full-wave simulator HFSS. A prototype operating at 5.7 GHz with a height of 0.069 λ_0 is designed, and the final design dimensions are included in the caption of Fig. 1. The simulated reflection coefficients and gains of the designed antenna element with different excitation ports are shown in Fig. 2. The simulated 10-dB return loss bandwidth is from 5.05 to 6.3 GHz, approximately 21.9% fractional bandwidth. The simulated gains are stable over the whole operating frequency band, and the cross-polarization level is lower than −30 dB. Simulated radiation patterns of the antenna element at 5.7 GHz are plotted in Fig. 3(a) and (b) for excitation at port 1 and 2, respectively, where co-polarization and cross-polarization components at E- and H-plane are included for comparison. Simulated results show that the antenna properties are almost identical for the two feeding ports. However, it
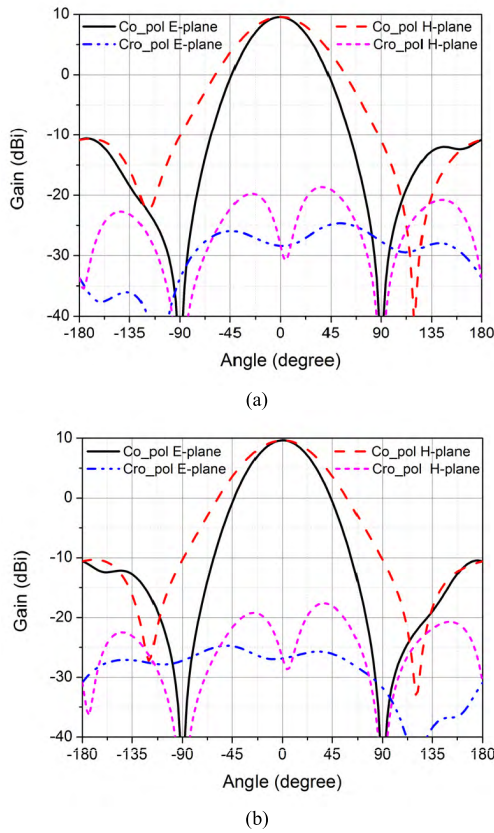
FIGURE 3. Simulated radiation patterns of the antenna element for the two different feeding ports. (a) Excitation at port 1; (b) Excitation at port2.

FIGURE 4. Simulated surface current distributions on the parasitic patch at two different time phases for the two feeding ports at 5.7-GHz. (a) Excitation at port 1; (b) Excitation at port 2.
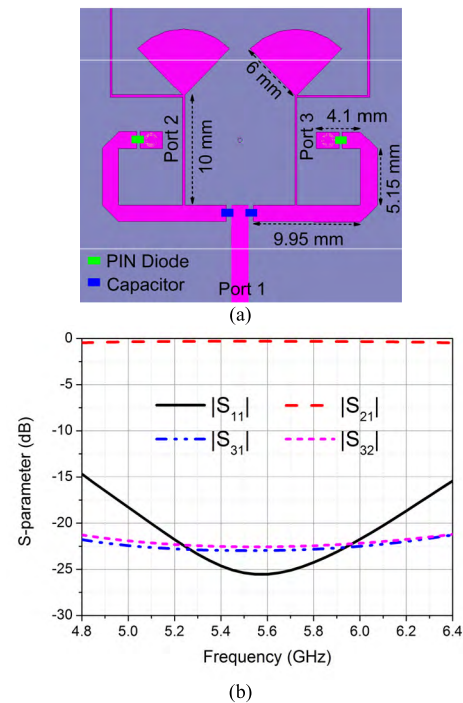
FIGURE 5. Layout and simulated results of the designed SPDT switch. (a) Layout; (b) Simulated results (port 2 on and port 3 off).

should be noted that a 180° phase difference between the two feeding ports exists due to the structural symmetry.

In order to see the 180° phase-difference characteristic of the proposed antenna element for the two feeding ports, the simulated surface current distributions on the parasitic patches are illustrated in Fig. 4. For the two excitations at the respective ports, the current vectors are opposite, which clearly demonstrates the 180° phase-difference between the two feeding ports. It can be concluded that the proposed antenna element exhibits good performance and produces two phase states, i.e., $\theta + 0°$ and $\theta + 180°$, respectively. Hence, the antenna element at each state can be considered as a basic digital element, mimicking the '0' (state 1) and '1' (state 2) for 1-bit. For example, the excitation at port 1 represents the '0' state and the port 2 denotes the '1' state. In the implementation, a 1-bit digital programmable antenna element is developed using a SPDT switch.

The SPDT switch is designed and integrated with the antenna element to switch between the two feeding ports. The layout and simulated results of the SPDT switch are shown in Fig. 5. Two p-i-n diodes (MADP-000907-14020) from MACOM [23] and two 2-pF capacitors from Murata are used. To control the SPDT switch, a dc voltage is supplied to the p-i-n diodes through a biasing circuit using a thin microstrip line as the inductor and a fan-shaped sector microstrip as

the shorting capacitor, as shown in Fig. 5(a). By parameter-tuning in the HFSS software, the SPDT switch achieves good performance in terms of isolation and insertion loss within the frequency band of 4.8-6.4 GHz. The final design parameters are marked in the layout. The simulated input–output and output–output isolations are higher than 22 dB, and the return loss is higher than 15 dB in the operating frequency band.

(a)

(b)

FIGURE 6. Layout of the antenna elements used to investigate the mutual coupling effect along (a) E-plane and (b) H-plane.

FIGURE 7. Mutual couplings of the antenna elements at the E- and H-plane.

The simulated results show that the SPDT switch is capable of switching the feeding port for the 1-bit antenna element.
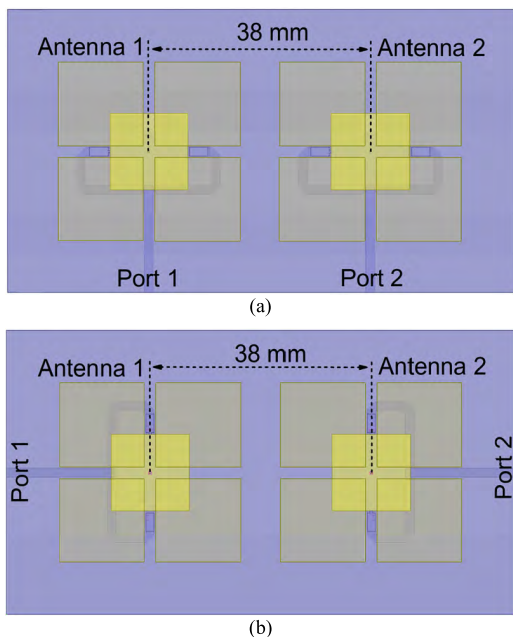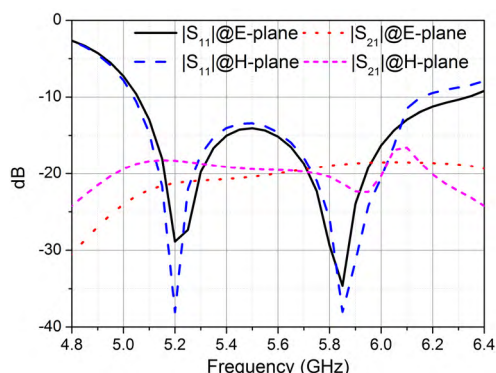
B. 4 × 4 ARRAY ANTENNA

Firstly, to study the mutual couplings between antenna elements, the proposed antenna elements are positioned along the E- and H-plane with the same center-to-center separation of 38 mm, as shown in Fig. 6. Fig. 7 shows the simulated mutual couplings of the antenna elements at the E- and H-plane, which exhibits the coupling level of less than −17 dB in both E- and H-plane over the whole operating frequency band.

Then, based on the proposed 1-bit antenna element, a 4 × 4 low profile wideband patch array antenna with dynamically tunable radiation beam is developed. Fig. 8(a) shows the top view of the array antenna. The 16 antenna elements are positioned with an inter-element spacing of 38 mm ($0.72\lambda_0$ at 5.7 GHz). The bottom view of the array antenna
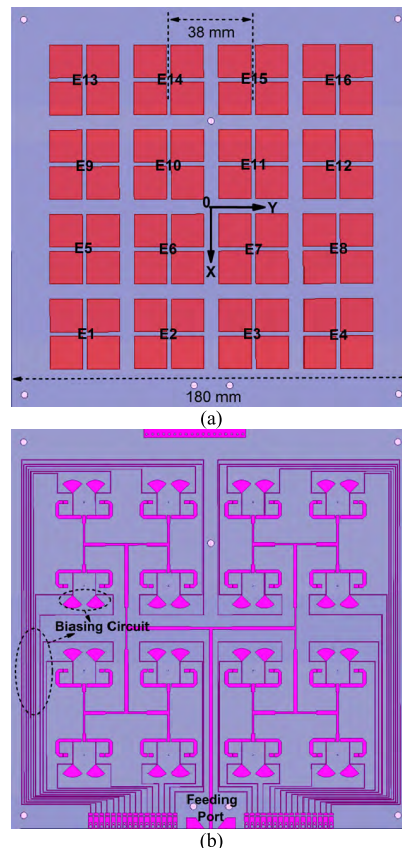

(a)

(b)

FIGURE 8. Layout of the proposed antenna array. (a) Top view. (b) Bottom view.

is depicted in Fig. 8(b), showing the 16-way power divider integrated with SPDT switches and the dc biasing circuits. Each antenna element can be independently controlled, and the radiation beams of the array antenna can be dynamically switched through different coding sequences of '0' and '1'. The simulated 3D radiation patterns of the proposed array antenna under different coding sequences are shown in Fig. 9, where the '0' state and '1' state are represented by the black and white patch, respectively. Sum beam, difference beams, two- and four-beam splitting can be achieved through spatial mixtures of these 1-bit digital antenna elements. For example, when the coding sequence of *E1~E16* is set as 0000000000000000, a sum beam can be generated in the far-field as shown in Fig. 9(a), whereas under the coding sequence of 0011001100110011, a difference beam can be achieved as seen in Fig. 9(b). Two-beam splitting as shown in Fig. 9 (d)-(e) and (h)-(m) and four-beam splitting as shown in Fig. 9(f) and (g) are also produced by proper coding sequences. It is worth noting that each radiation beam pattern can also be generated by the corresponding complementary coding sequence.

III. EXPERIMENTS AND MEASUREMENT RESULTS

To validate the simulated results, the designed 1-bit digital-controllable array antenna has been prototyped
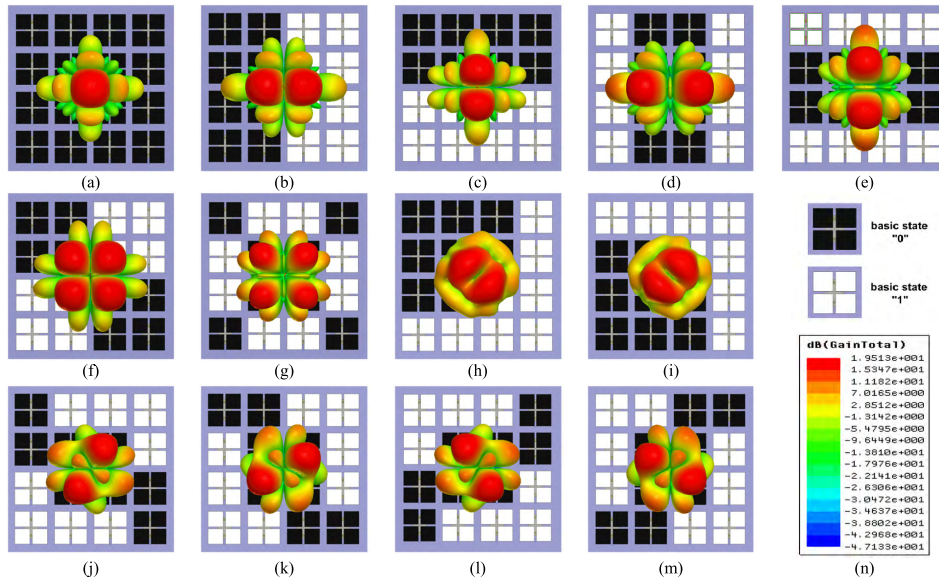
FIGURE 9. Simulated far-field 3D radiation beams of the proposed 1-bit digital array antenna under different coding sequences at the center frequency of 5.7 GHz. (a) Mode 1 (0000000000000000). (b) Mode 2 (0011001100110011). (c) Mode 3 (0000000011111111). (d) Mode 4 (1001100110011001). (e) Mode 5 (1111000000001111). (f) Mode 6 (1100110000110011). (g) Mode 7 (0110100110010110). (h) Mode 8 (1111001100010001). (i) Mode 9 (0001000100111111). (j) Mode 10 (1110100000010111). (k) Mode 11 (1100100110010011). (l) Mode 12 (0111000110001110). (m) Mode 13 (0011100110011100). (n) Color scale.
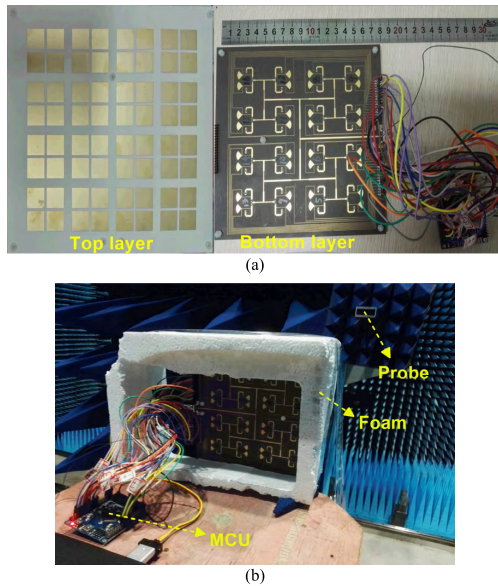

FIGURE 10. (a) Photograph of the antenna prototype. (b) The measurement setup.

FIGURE 11. Measured reflection coefficients of the fabricated array antenna at different states.

and measured. The photograph of the fabricated prototype is shown in Fig. 10(a). M3 nylon bolts and plastic washers with a thickness of 2 mm are used to support the parasitic patch layer. In measurement, a MCU hardware (STM32F103V8) [24] is used to digitally control the coding sequences. The reflection coefficients of the proposed digital-controllable array antenna under different coding sequences are measured by Agilent Vector Network Analyzer (VNA), and the results are plotted in Fig. 11. It can be observed that

the measured 10-dB return loss bandwidths for all modes cover a wide frequency band from 5.12 to 6.32 GHz, approximately 21.4% fractional bandwidth.

The radiation properties under different coding sequences are measured in microwave anechoic chamber using a near-field test method [25]. A photograph of the measurement setup is shown in Fig. 10(b). The far-field radiation patterns are obtained through the near-field to far-field transformation. The measured 5.7 GHz 3D normalized radiation beams under different coding sequences are illustrated in Fig. 12. From Fig. 9 and 12, it can be observed that the measured results agree well with the simulated results.

The measured and simulated far-field radiation patterns at corresponding cut-planes are compared at 5.7 GHz, as shown in Fig. 13-16. The results for Mode 1 are compared at both

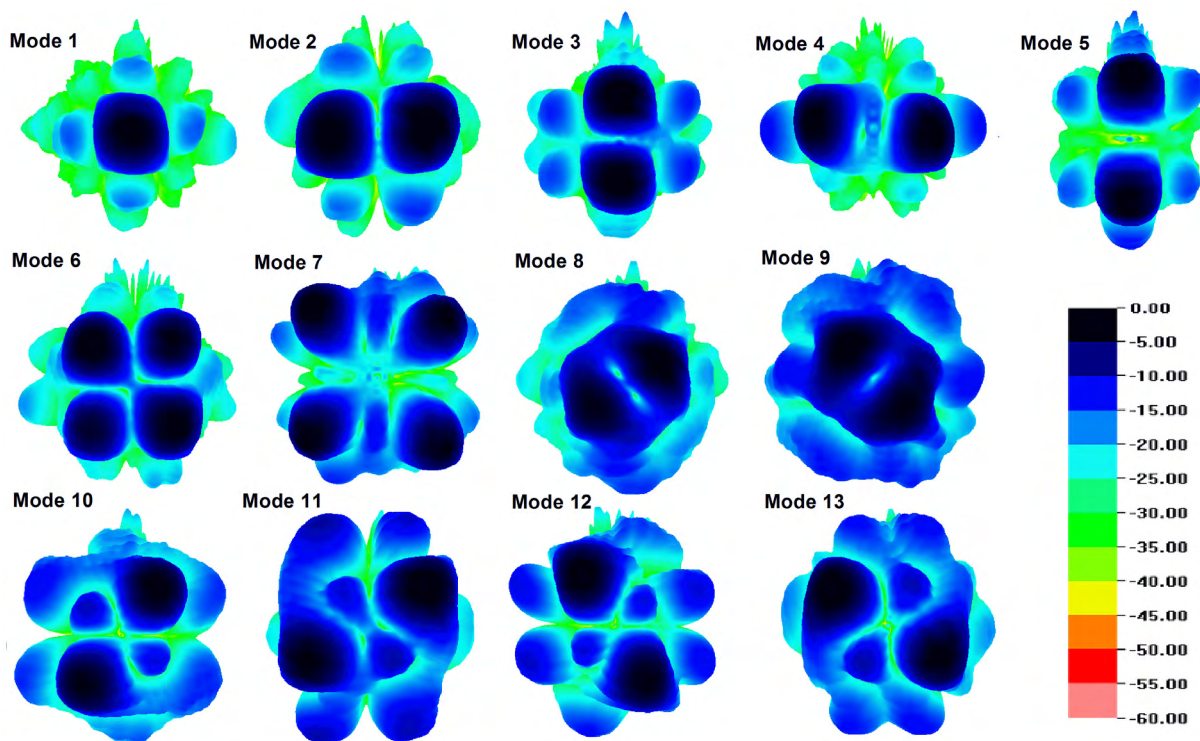**FIGURE 12.** Measured 5.7 GHz normalized 3D radiation beams of the proposed 1-bit digital array antenna under different coding sequences.
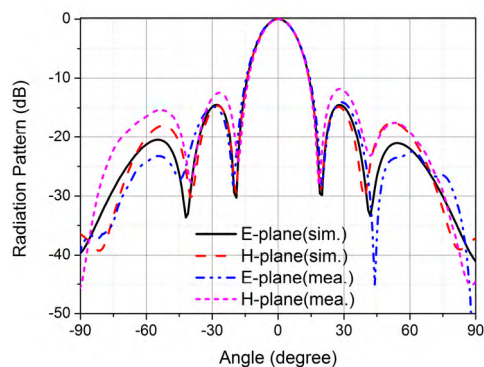

FIGURE 13. Measured and simulated 5.7 GHz normalized radiation patterns of the array antenna for Mode 1.
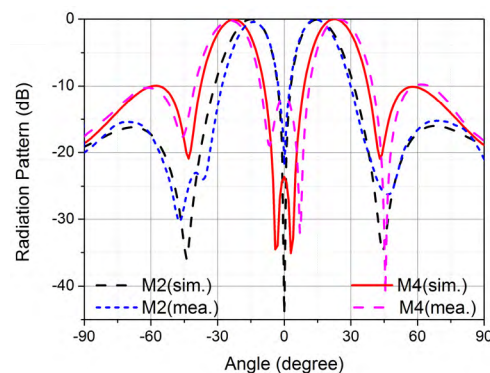

FIGURE 14. Measured and simulated 5.7 GHz E-plane normalized radiation patterns of the array antenna for Mode 2 and Mode 4.

E- and H-plane, showing a close agreement between the simulation and experiment. It is worthwhile to point out here that the Mode 1-3 can be used as a monopulse antenna, where Mode 1 produces a sum beam, and Mode 2-3 produce two difference beams. The measured null-depth for Mode 2 and Mode 3 are −22.5 dB and −23 dB, respectively. For Mode 6 and Mode 7, four beams can be produced in the four quadrants, $\phi = 45°$, 135°, 225° and 315°. The radiation patterns at these two cut-planes are drawn in Fig. 16. The measured half power beam-widths (HPBWs) and beam direction for Mode 1-7 at 5.7 GHz have been listed in Table 1. As confirmed in Fig. 13-16, the measured results are in good

agreement with the simulation except that the measured null-depths are higher than the simulated results. This is caused by the relatively low isolation between the output ports of the SPDT. This can be improved by adopting a higher isolation switch, such as a MEMS switch.

To view the radiation performance over the whole operating frequency band, the measured far-field radiation patterns versus angle and frequency for the Mode 1-3 are illustrated in Fig. 17-19. The measured radiation patterns for Mode 1 (sum beam) at the E- and H-plane are plotted in Fig. 17, which clearly shows that the radiation pattern is stable over the operating frequency band of 5.1-6.3 GHz. The difference
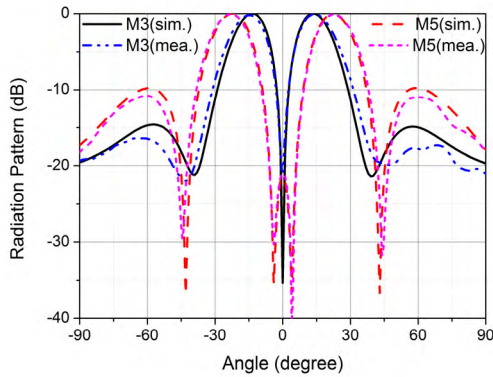
FIGURE 15. Measured and simulated 5.7 GHz H-plane normalized radiation patterns of the array antenna for Mode 3 and Mode 5.
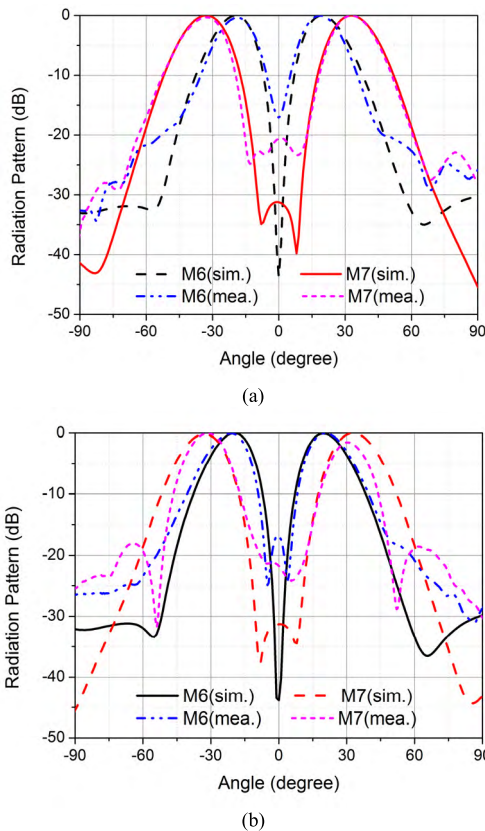

(a)

(b)

FIGURE 16. Measured and simulated 5.7 GHz normalized radiation patterns of the array antenna for Mode 6 and Mode 7. (a) 45-degree plane. (b) 135-degree plane.

TABLE 1. Measured HPBWs and beam direction for mode 1-7.

	Beam number	Beam direction (φ, θ)	HPBWs
Mode 1	One beam in boresight direction	(0°, 0°)	16°
Mode 2	Two beams in φ=90°,270°	(90°, 14°) (270°,14°)	14.5° 15.5°
Mode 3	Two beams in φ=0°,180°	(0°, 14.5°) (180°, 14.5°)	16° 16°
Mode 4	Two beams in φ=90°,270°	(90°, 24.5°) (270°, 24.5°)	17.5° 17.5°
Mode 5	Two beams in φ=0°,180°	(0°, 23.5°) (180°, 23.5°)	16.5° 16.5°
Mode 6	Four beams in φ=45°, 135°, 225°,315°	(45°, 18.5°) (135°, 18.5°) (225°, 18.5°) (315°, 18.5°)	15.5° 17° 16.5° 16.5°
Mode 7	Four beams in φ=45°, 135°, 225°,315°	(45°, 32.5°) (135°, 32.5°) (225°, 32.5°) (315°, 32.5°)	18° 16.5° 17.5° 13.5°

(a)

(b)
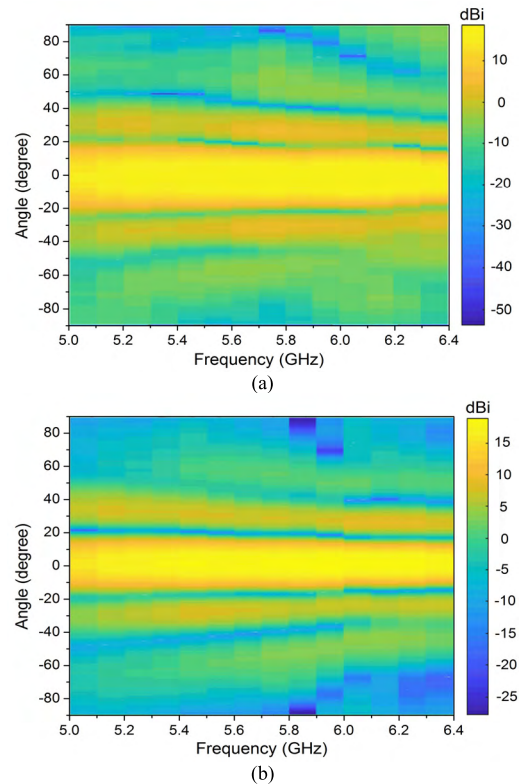
FIGURE 17. Measured radiation patterns as a function of frequency for Mode 1. (a) E-plane. (b) H-plane

beams at the H-plane (Mode 2) and E-plane (Mode 3) are shown in Fig. 18 and Fig. 19, respectively. The traditional 180° phase shifter, in the form of a half-wavelength transmission line, has a narrow frequency band. When the operating frequency departures the center frequency, the prescribed phase difference cannot be satisfied. So, the null-angle will normally deviate slightly from the boresight direction. Here, no deviation of the null-angle is observed at the boresight direction over the broad operating frequency band due to the

symmetrical structure used, as confirmed in Fig. 17-19. It can be concluded that the radiation gains and null-depth are stable over the whole operating bandwidth for Mode 1-3, which can be used as a monopulse antenna.

The measured gain and radiation efficiency at the boresight direction for the sum beam (Mode 1) are presented in Fig. 20, where the simulated results are also presented for comparison. The measured peak gain, including the loss of the feeding network, SPDT switches, SMA connectors, and conductors,
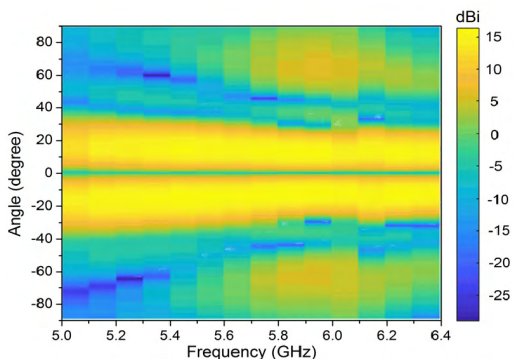
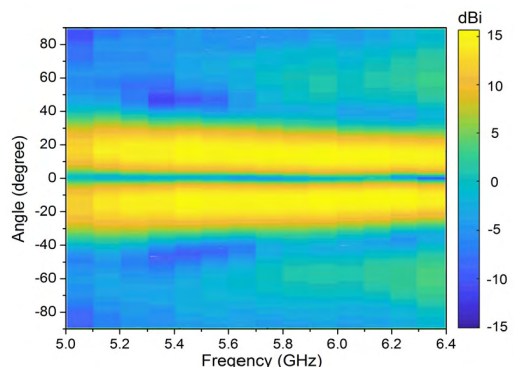**FIGURE 18.** Measured radiation patterns as a function of frequency for Mode 2.

FIGURE 19. Measured radiation patterns as a function of frequency for Mode 3.
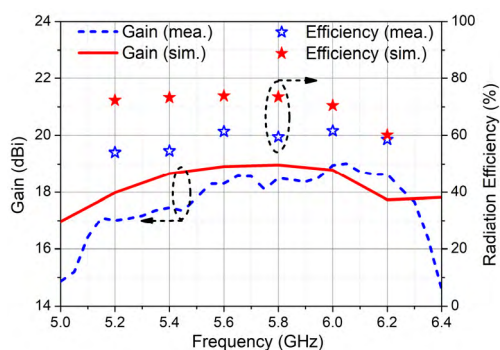

FIGURE 20. Measured and simulated gain and radiation efficiency of the fabricated antenna for the sum beam (mode 1).

achieves 19 dBi at 6 GHz and the 3-dB gain bandwidth is from 5.1 to 6.35 GHz, approximately 21.9% fractional bandwidth. This indicates that the measured gain is stable over a wide frequency band. The measured radiation efficiency, which is obtained by calculating the ratio of the measured gain to the simulated directivity, is around 60% within the whole operating frequency band. Due to the symmetrical structure, the radiation efficiency for other modes is similar with that for the sum beam.

Finally, comparisons between previously reported beam switchable antennas and this work are made in Table 2.

TABLE 2. Performance comparison with previously reported beam switchable antennas.

	This work	[11]	[12]	[13]	[14]
Operating frequency (GHz)	5.7	2.4	2.45	2.4	2.9
Bandwidths (%)	21	1.25	2	6.25	3.4
No. of available beams	13	12	8	4	4
Scanning range (°)	65	86	n. a.	72	56
Maximum Gain (dBi)	19	8.2	13	5.34	7.2
Polarization	LP	LP	LP	LP	LP
Profile (λ_0)	0.069	0.012	0.1	0.05	0.08

It is evident that the proposed pattern reconfigurable patch antenna array in this work exhibits the widest impedance bandwidth and the highest peak gain. It also has the ability to control radiation beams, including single radiation beam, double radiation beams as well as multiple radiation beams. In addition, the beams are stable over the whole operating frequency band due to the symmetrical structure. This shows that the proposed antenna has the flexibility in manipulating the radiation beams over a wide frequency band.

IV. CONCLUSION

In this paper, a wideband 1-bit 4×4 digital-controllable patch array antenna with dynamic beam manipulation capability is developed. It consists of 16 1-bit antenna elements. The operating bandwidths are broadened by adopting a stacked patch structure and the probe-fed technique. The code of each antenna element can be independently controlled, and the radiation beams of the array antenna can be dynamically switched through different coding sequences using a MCU. Multiple radiation beams including sum beam, difference beams as well as quad-beams can be achieved. A prototype of array antenna is fabricated and tested under different coding sequences. The measured results agree well with the simulated results. The proposed array antenna shows the capability of powerful dynamic beam manipulation, wide operating bandwidth, and the ease of design and fabrication.

REFERENCES

[1] H. L. Zhu, X. H. Liu, S. W. Cheung, and T. I. Yuk, "Frequency-reconfigurable antenna using metasurface," *IEEE Trans. Antennas Propag.*, vol. 62, no. 1, pp. 80–85, Jan. 2014.

[2] J. Hu, Z.-C. Hao, and W. Hong, "Design of a wideband quad-polarization reconfigurable patch antenna array using a stacked structure," *IEEE Trans. Antennas Propag.*, vol. 65, no. 6, pp. 3014–3023, Jun. 2017.

[3] J. Hu, G. Q. Luo, and Z.-C. Hao, "A wideband quad-polarization reconfigurable metasurface antenna," *IEEE Access*, to be published.

[4] M. A. Y. Abdalla, K. Phang, and G. V. Eleftheriades, "A planar electronically steerable patch array using tunable PRI/NRI phase shifters," *IEEE Trans. Microw. Theory Techn.*, vol. 57, no. 3, pp. 531–541, Mar. 2009.

[5] L. Boccia, I. Russo, G. Amendola, and G. D. Massa, "Multilayer antenna-filter antenna for beam-steering transmit-array applications," *IEEE Trans. Microw. Theory Techn.*, vol. 60, no. 7, pp. 2287–2300, Jul. 2012.

[6] H. Li *et al.*, "Reconfigurable diffractive antenna based on switchable electrically induced transparency," *IEEE Trans. Microw. Theory Techn.*, vol. 63, no. 3, pp. 925–936, Mar. 2015.

[7] C. Huang, W. Pan, X. Ma, B. Zhao, J. Cui, and X. Luo, "Using reconfigurable transmitarray to achieve beam-steering and polarization manipulation applications," *IEEE Trans. Antennas Propag.*, vol. 63, no. 11, pp. 4801–4810, Nov. 2015.

[8] Z.-C. Hao, H.-H. Wang, and W. Hong, "A novel planar reconfigurable monopulse antenna for indoor smart wireless access points' application," *IEEE Trans. Antenna Propag.*, vol. 64, no. 4, pp. 1250–1261, Apr. 2016.

[9] S. Xiao, C. Zheng, M. Li, J. Xiong, and B.-Z. Wang, "Varactor-loaded pattern reconfigurable array for wide-angle scanning with low gain fluctuation," *IEEE Trans. Antennas Propag.*, vol. 63, no. 5, pp. 2364–2369, May 2015.

[10] P. Lotfi, S. Soltani, and R. D. Murch, "Broadside beam-steerable planar parasitic pixel patch antenna," *IEEE Trans. Antenna Propag.*, vol. 64, no. 10, pp. 4519–4524, Oct. 2016.

[11] A. Pal, A. Mehta, D. Mirshekar-Syahkal, and H. Nakano, "A twelve-beam steering low-profile patch antenna with shorting vias for vehicular applications," *IEEE Trans. Antennas Propag.*, vol. 65, no. 8, pp. 3905–3912, Aug. 2017.

[12] M. S. Sharawi, S. Deif, and A. Shamim, "An electronically controlled 8-element switched beam planar array," *IEEE Antennas Wireless Propag. Lett.*, vol. 14, pp. 1350–1353, Feb. 2015.

[13] M. S. Alam and A. M. Abbosh, "Beam-steerable planar antenna using circular disc and four pin-controlled tapered stubs for WiMAX and WLAN applications," *IEEE Antennas Wireless Propag. Lett.*, vol. 15, pp. 980–983, 2016.

[14] Y. Y. Bai, S. Xiao, C. Liu, X. Shuai, and B. Z. Wang, "Design of pattern reconfigurable antennas based on a two–Element dipole array model," *IEEE Trans. Antenna Propag.*, vol. 61, no. 9, pp. 4867–4871, Sep. 2013.

[15] S. V. Hum and J. Perruisseau-Carrier, "Reconfigurable reflectarrays and array lenses for dynamic antenna beam control: A review," *IEEE Trans. Antennas Propag.*, vol. 62, no. 1, pp. 183–198, Jan. 2014.

[16] H. Yang *et al.*, "A 1600-element dual-frequency electronically reconfigurable reflectarray at X/Ku-band," *IEEE Trans. Antennas Propag.*, vol. 65, no. 6, pp. 3024–3032, Jun. 2017.

[17] C. Huang, W. Pan, and X. Luo, "Low-loss circularly polarized transmitarray for beam steering application," *IEEE Trans. Antennas Propag.*, vol. 64, no. 10, pp. 4471–4476, Oct. 2016.

[18] L. Di Palma, A. Clemente, L. Dussopt, R. Sauleau, P. Potier, and P. Pouliguen, "Radiation pattern synthesis for monopulse radar applications with a reconfigurable transmitarray antenna," *IEEE Trans. Antennas Propag.*, vol. 64, no. 9, pp. 4148–4154, Sep. 2016.

[19] T. J. Cui, M. Q. Qi, X. Wan, J. Zhao, and Q. Cheng, "Coding metamaterials, digital metamaterials and programmable metamaterials," *Light-Sci. Appl.*, vol. 3, no. 10, p. e218, Oct. 2014.

[20] X. Wan, M. Q. Qi, T. Y. Chen, and T. J. Cui, "Field-programmable beam reconfiguring based on digitally-controlled coding metasurface," *Sci. Rep.*, vol. 6, Feb. 2016, Art. no. 20663.

[21] C. Huang, B. Sun, W. Pan, J. Cui, X. Wu, and X. Luo, "Dynamical beam manipulation based on 2-bit digitally-controlled coding metasurface," *Sci. Rep.*, vol. 7, p. 42302, Feb. 2017.

[22] J. Hu and Z.-C. Hao, "A wideband antenna with switchable beams," in *Proc. IEEE MTT-S Int. Microw. Conf.*, Honolulu, HI, USA, Jun. 2017, pp. 850–852.

[23] MACOM. *MADP-000907-14020P PIN Diode*. Accessed: 2015. [Online]. Available: http://www.macom.com/products/product-detail/MADP-000907-14020P

[24] STMicroelectronics. *STM32F103V8*. Accessed: 2015. [Online]. Available: http://www.st.com/content/st_com/en/products/microcontrollers/stm32-32-bit-arm-cortex-mcus/stm32-mainstream-mcus/stm32f1-series/stm32f103/stm32f103v8.html

[25] C. A. Balanis, *Antenna Theory: Analysis and Design*. Hoboken, NJ, USA: Wiley, 2016.
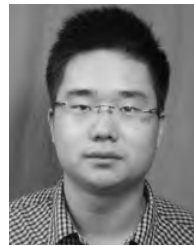
JUN HU (S'17) received the B.S. degree in electronics and information engineering from Anhui Agricultural University, Hefei, China, in 2012, and the M.S. degree in electromagnetic field and microwave technology from Southeast University, Nanjing, China, in 2014, where he is currently pursuing the Ph.D. degree in electronic science and technology.

His recent research interests include the design of tunable devices, passive components, reconfigurable antennas, and antenna array.

ZHANG-CHENG HAO (M'08–SM'15) received the B.S. degree in microwave engineering from Xidian University, Xi'an, China, in 1997, and the M.S. and Ph.D. degrees in radio engineering from Southeast University, Nanjing, China, in 2002 and 2006, respectively. In 2006, he was a Post-Doctoral Researcher with the Laboratory of Electronics and Systems for Telecommunications, École Nationale Supérieure des Télécommunications de Bretagne, Bretagne, France, where he was involved in developing millimeter-wave antennas. In 2007, he joined the Department of Electrical, Electronic and Computer Engineering, Heriot-Watt University, Edinburgh, U.K., as a Research Associate, where he was involved in developing multilayer integrated circuits and ultrawideband components. In 2011, he joined the School of Information Science and Engineering, Southeast University, as a Professor. He holds 20 granted patents and he has authored and co-authored over 150 referred journal and conference papers. His current research interests include microwave and millimeter-wave systems, submillimeter-wave and terahertz components, and passive circuits, including filters, antenna arrays, couplers, and multiplexers.

Dr. Hao has served as a reviewer for many technique journals, including the IEEE TRANSACTIONS ON MICROWAVE THEORY AND TECHNIQUES, the IEEE TRANSACTIONS ON ANTENNAS AND PROPAGATION, the IEEE ANTENNAS AND WIRELESS PROPAGATION LETTERS, and the IEEE MICROWAVE AND WIRELESS COMPONENTS LETTERS. He was a recipient of the Thousands of Young Talents presented by China Government in 2011 and the High-Level Innovative and Entrepreneurial Talent presented by Jiangsu, China, in 2012.

YI WANG (M'09–SM'12) was born in Shandong, China. He received the B.Sc. degree in physics and M.Sc. degree in condensed matter physics from the University of Science and Technology, Beijing, China, in 1998 and 2001, respectively, and the Ph.D. degree in electronic and electrical engineering from the University of Birmingham, Birmingham, U.K., in 2005.

In 2004, he was a Research Fellow at the University of Birmingham involved in high-frequency device applications of novel materials and structures. From 2011 to 2017, he was a Senior Lecturer and Reader with the University of Greenwich, U.K. He is currently a Senior Lecturer with the University of Birmingham. His present research interests include multi-role microwave circuits and their co-design, antennas, micromachining, millimeter-wave, and terahertz devices for metrology, communications, sensors, millimeter-wave measurements, and material characterizations.

● ● ●